Journal Pre-proof

A Programmable Compound Prism Powered by Triboelectric Nanogenerator for Highly Efficient Solar Beam Steering

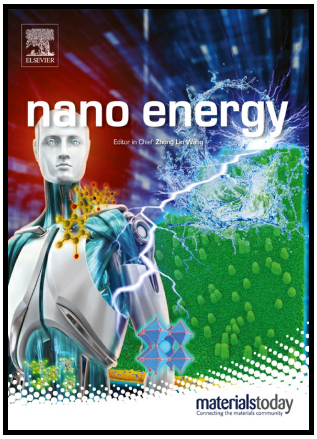

Guijun Chen, Yutao Wang, Dongyue Jiang, Hongchen Wang, Kun Wang, Jie Tan, Mingyang Sun, Yongchen Song, Minyi Xu

PII: S2211-2855(20)31098-3

DOI: https://doi.org/10.1016/j.nanoen.2020.105524

Reference: NANOEN105524

To appear in: *Nano Energy*

Received date: 2 September 2020
Revised date: 14 October 2020
Accepted date: 20 October 2020

Please cite this article as: Guijun Chen, Yutao Wang, Dongyue Jiang, Hongchen Wang, Kun Wang, Jie Tan, Mingyang Sun, Yongchen Song and Minyi Xu, A Programmable Compound Prism Powered by Triboelectric Nanogenerator for Highly Efficient Solar Beam Steering, *Nano Energy,* (2020) doi:https://doi.org/10.1016/j.nanoen.2020.105524

A Programmable Compound Prism Powered by Triboelectric Nanogenerator for Highly Efficient Solar Beam Steering

Guijun Chen[a,#] , Yutao Wang[a,#], Dongyue Jiang[a,*], Hongchen Wang[a], Kun Wang[a], Jie Tan[a], Mingyang Sun[a], Yongchen Song[a], Minyi Xu[b]

[a]Key Laboratory of Ocean Energy Utilization and Energy Conservation of Ministry of Education, Dalian University of Technology, China 116024

[b]Marine Engineering College, Dalian Maritime University, Liaoning Province, China 116026

Abstract

Concentrator photovoltaics (CPV) has great competitiveness in replacing the conventional flat-panel PV system due to its high conversion efficiency and small cell active area. However, the accessory beam steering and concentrating optics are bulky and costly. Here we propose a programmable compound prism (PCP) powered by triboelectric nanogenerator (TENG) for solar beam steering. A disc TENG with a RC circuit could produce DC voltage signal, and the voltage signal could be tuned by varying the resistance in RC circuit. By connecting the variable DC output to the left, right and back walls of the PCP filled with DC 550 silicone oil, DI water and PMX 200 silicone oil, the two oil/water interfaces could be modulated in a programmable manner. A maximum deflection angle range of 15° was achieved in the PCP, which is 38% greater than conventional single prism with only one oil/water interface. The proposed TENG-PCP was employed to deflect an oblique incident laser beam to trigger the power generation in a multi-junction solar cell. With the operation of the proposed TENG-PCP, a 1.2 mW increment was achieved by the multi-junction solar cell, indicating the potential of boosting the CPV by the presented TENG-PCP.

Graphical Abstract

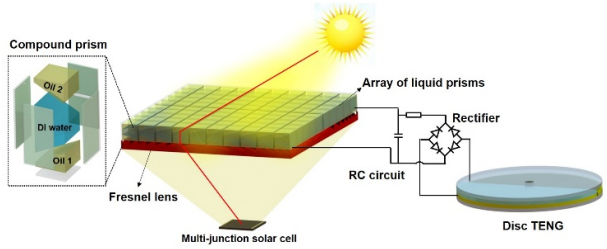

A programmable compound prism array powered by TENG deflecting the oblique incident solar beam for power generation in CPV.

Keywords: **TENG; Multi-phase flow; Concentrator photovoltaics; Beam steering**

* Corresponding author, Email: jiangdy@dlut.edu.cn; # These two authors contribute equally to this work.

1. Introduction

Concentrator photovoltaics (CPV) using multi-junction solar cells and concentrating optics is of great potential for applications in the utility-scale segment and high insolation areas [1-3]. As compared to the conventional flat-panel PV system, two obvious advantages are ahead of CPV technology including high conversion efficiency and small active area. The high conversion efficiency arises from sunlight concentration as well as the multi-junction cell. The highly concentrated sunlight has led to a higher density of photo-generated carriers for driving a larger quasi-Fermi-level splitting in the semiconductor material, thus enabled an increased output voltage [4]. On the other hand, the multi-junction solar cell allows for the absorbance of a wider range of wavelength and improves the sunlight to electrical conversion efficiency [5-7]. A lab-scale example has demonstrated over 46% conversion efficiency under 508 Suns irradiance, which is a world record value achieved in 2014 [8]. These advantages open up opportunities for reducing the cost per watt of manufacturing capital, doubling the usage of land area and preventing large fluctuations in module price. However, in order to maintain the performance of the CPV system, the multi-junction solar cell needs to be mounted to solar concentrators and trackers to ensure orientation normal to the incident light. The additional cost and land occupation of the concentrators, trackers and coolers have greatly weakened the advantages of the CPV system even though a higher conversion efficiency and smaller cell area could be expected (theoretical limiting efficiency of 86.8% under highly concentrated sunlight [9]).

Several solar tracking strategies have been proposed for CPV applications including: single/dual axis rotational tracking, beam steering, planar micro-tracking and luminescent tracking [10-14]. Among these tracking strategies, both rotational tracking and planar micro-tracking require a mechanical tracker for moving either the concentrating optics or the multi-junction cell to the location of the light, which would incur additional investment and annual maintenance cost to the system (US$0.36-0.38$W^{-1}$ on average) [15, 16]. As a comparison, the beam steering solar tracking strategy is of great potential as it is free of external mechanical tracker, which reduces the initial investment and maintenance cost. Besides, the beam steering technology is able to integrate with conventional concentrating elements (e.g. Fresnel lens) to achieve high concentrations. These features allow the CPV system to be roof-top compatible and cost competiveness with flat-panel PVs [17]. As a candidate technology for next-generation beam steering, electrowetting-on-dielectric based liquid prisms have been widely investigated [18-20]. In a liquid prism device, bias voltage is applied to the different walls of the prism for modifying the surface energy, thus leading to the dynamic movement of the water and oil interface [21]. The movement of the water and oil interface always ensures a vertical outgoing beam no matter the sunlight shines at negative or positive incident angles. The conventional liquid prisms face two major challenges. The first challenge originates from the usage of DC power source. The DC power source in the system not only increases the capital investment, but also adds on annual maintenance cost. It is desired to develop a self-powered or environmental energy powered liquid prism beam steering device. The second challenge is the selection of the immiscible fluids in the liquid prism. The

requirement on immiscibility, refractive indices and densities narrows down the available liquid options, thus the single prism with a pair of immiscible liquids is intensively investigated. In the single prism, only one dynamic interface is used for beam steering and the maximum deflection angle is limited [22].

Since the first report of triboelectric nanogenerator (TENG) by Wang's group [23-25], TENG devices have been recognized as a good candidate to scavenge the arbitrary mechanical energy from nature and environment [26-32] and the output performance has been boosted rapidly [33-36]. The harvested energy has been demonstrated for powering small-scale electronics and promoted the development of self-powered systems [37-46]. Several TENG triggered optical systems have successfully demonstrated the functions of mechanical motion monitoring [47], varifocal [48], transmittance and grating modulation [49-51]. These systems have shown great potential in the design of self-powered optical system. However, the studies on the TENG powered dynamic beam steering devices require further exploration. Herein we propose a TENG powered programmable compound prism (PCP) for beam steering which could be potentially used in concentrator photovoltaics. As compared to the conventional liquid prisms and TENG powered optical systems, the TENG-PCP provides the advantages of: i) the PCP is powered by a TENG device with RC circuit, which eliminates the employment of DC power sources and reduces both the capital and maintenance costs; ii) the beam steering device is achieved by a programmable compound prism which has two dynamic water/oil interfaces and allows for a dynamic beam steering at wider acceptance angle of incident lights (~15°), which is 38% greater than that of conventional single prism. The usage of TENG-PCP for deflecting a laser beam to power a $GaInP_2$/GaAs/Ge multi-junction solar cell was demonstrated and 1.2 mW solar cell power was boosted by the TENG-PCP.

2. Results and Discussion

2.1 Concept and working principle of the TENG-PCP.

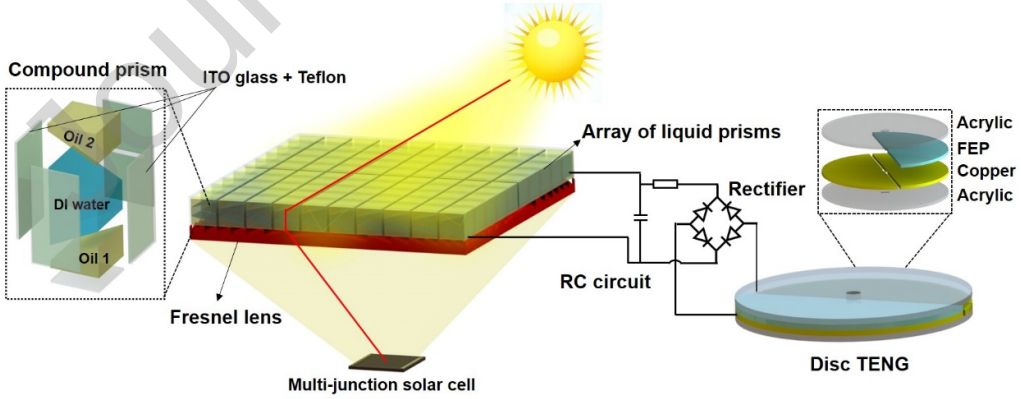

Figure 1 Concept of the TENG-PCP beam steering system for CPV applications. The system is composed of a disc TENG with RC circuit, array of PCPs, a Fresnel lens and multi-junction PV cell. The oblique incident sunlight is steered by the liquid prism which is driven by a disc TENG device. The Fresnel lens concentrates the steered sunlight for power generation by a multi-junction ($GaInP_2$/InGaAs/Ge) solar cell.

Figure 1 illustrates the concept of a TENG driven solar beam steering device integrated with a Fresnel lens for CPV application. The system is composed of an array of PCPs, a Fresnel lens, a $GaInP_2$/InGaAs/Ge multi-junction cell and a disc TENG with RC circuit. The disc TENG device is formed by an acrylic cover, a commercial FEP film, a pair of copper electrodes and an acrylic substrate. When the disc TENG is rotating, the FEP film alternate contacts and separates with the copper electrodes. Such a rotating motion triggers contact electrification and electrostatic induction phenomena which leads to the movement of the transferred charges through the external circuit and the generation of an alternative electric signal between the copper electrodes. The full wave rectifier and RC circuit (formed by a resistor and a capacitor) convert the AC signal into a DC one. The DC electric potential could be used to provide power to actuate the oil/water interfaces in the PCP. The PCP (details of fabrication could be found from Figure S1 in Supporting Information) is a glass container filled with immiscible liquids. The left, right and back walls of the PCP are Teflon AF (Teflon amorphous fluoropolymer, details of the preparation process could be found from the Materials and Methods section) coated ITO glass. The ITO on the left and right walls plays a role as the actuation electrode, while the ITO on the back wall of the PCP is used as a ground electrode. The front wall is a piece of bare glass coated with Teflon AF and base wall is a piece of bare glass without coating. The container is filled with a heavier oil (DC 550 silicone oil), DI water and a lighter oil (PMX 200 silicone oil). To form an EWOD circuit, the Teflon AF layer on the back wall was broken to be short-circuited with DI water. When the DC electric potential is connected with the side walls of the PCP, the meniscus between water and oil could be tuned to be positively or negatively forming programmable prism angles. As the refractive indices of the three liquids are different, the prism angle deflects the oblique incident light beam and guides the sunlight perpendicularly to the Fresnel lens. The light beam passes through the Fresnel lens could be concentrated to the surface of the multi-junction cell for power generation.

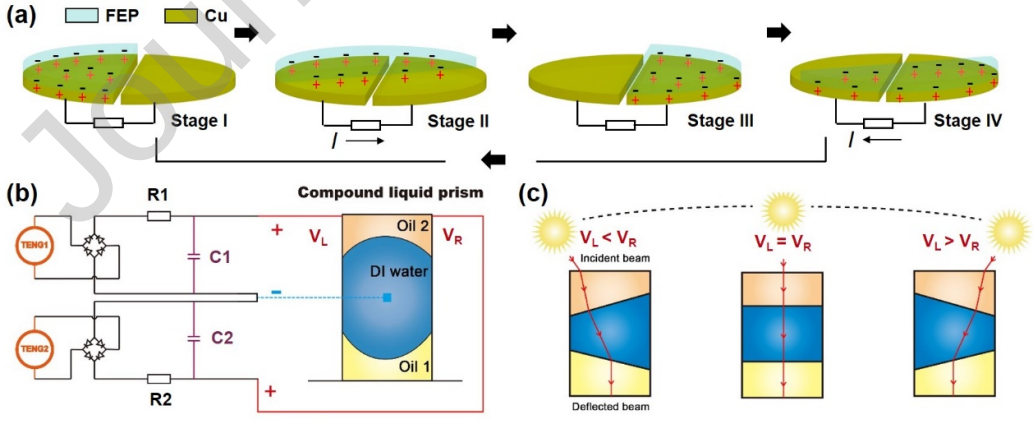

Figure 2 Working principle of the TENG powered beam steering system. (a) Movement of the triboelectric charges when the FEP film is rotating between the left and right copper electrodes. (b) Electric circuit of using the disc TENG for modulating the PCP. (c) Programmable beam steering mechanism by the compound prism.

Detailed working principle of the TENG-PCP is shown in Figure 2. As shown in Figure 2a (stage I), when the FEP film slides against the copper electrodes, the FEP surface possesses negative charges due to triboelectric effect. Initially, the FEP film is fully overlapped with the left electrode, the positive charges are attracted to the upper surface of the left electrode (stage I). When the FEP film is driven towards the right copper electrode (stage II), the positive charges will flow from the left electrode to the right electrode to screen the local field of the negative charges on the FEP film, thus generating a current flow. When the FEP film is driven to fully overlap with the right electrode (stage III), the positive charges are all attracted to the right electrode. When the FEP film is driven towards the left electrode, the flow of positive charges would induce a reverse current flow. With the continuous motion, a cycle between the stage I to stage IV is established and an alternate current can be detected between the two copper electrodes. Two DC voltage signals are required to drive the two walls of the PCP separately to achieve the straight interfaces. Figure 2b shows the detailed electric circuit of the TENG-PCP devices. The two disc TENGs are connected with rectifiers and RC circuits to obtain a direct current output signal. The positive terminals of the two disc TENGs after RC circuits are connected with left and right wall electrodes of the PCP, respectively. The negative terminals are connected to the ground electrode (back wall) of the PCP. By changing the resistance of the RC circuit, the left and right wall voltage applied to the PCP can be tuned. More details of the circuit model could be found from Figure S2 in Supporting Information. As shown in Figure 2c, when the left wall voltage V_L is smaller than the right wall voltage V_R, a trapezoid DI water shape could be obtained, while if the left wall voltage V_L is greater than the right wall voltage V_R, a flipped trapezoid DI water shape could be obtained. The variation of the DI water shape continuously changes the prism angle, which ensures a perpendicular outgoing beam no matter the sunlight is with a positive or negative incident angle. The control strategy of the PCP for a certain day could be achieved by timer controlled switch and the details could be found from Figure S3 in Supporting Information.

2.2 Output performance of the disc TENG device and prism angle modulation

Two disc TENGs were assembled with the same dimension: the diameter of the acrylic cover and substrate is 200 mm and the FEP film and copper electrodes are in a half-circle shape. A 5 mm gap is kept between the left and right copper electrodes. The rotating speed of the step motor is set as 100 rpm for pursuing a more stabilized output DC signal. The open-circuit voltage, short-circuit current and transferred charges during the operation of disc TENG is recorded in Figure 3a, 3b and 3c. A peak-to-peak open-circuit voltage of 530 V, short-circuit current of 1.2 μA and transferred charge of 140 nC is obtained. In the DC output performance test, a full rectifier, a resistor and a capacitor (0.1 μF) are employed. The capacitor helps stabilize the output DC signal while the resistor in the RC circuit plays a role as resistive divider. A larger resistance in the RC circuit would lead to a reduced voltage on the PCP. When the resistances vary from 500 MΩ to 10 GΩ, the voltage applied to the PCP are measured in the range of 88-197 V as shown in Figure 3d.

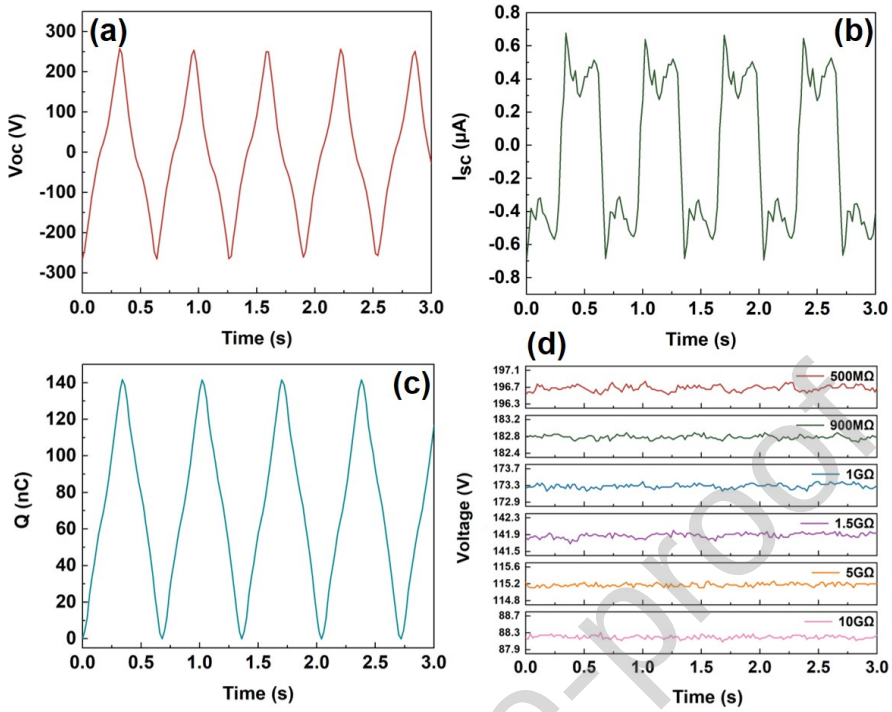

Figure 3. Output performance of the disc TENG with rectifier and RC circuit. (a) Open-circuit voltage (b) short-circuit current (c) transferred charges (d) DC voltage signal on the PCP varying with the resistance of the RC circuit.

Figure 4a illustrates an as prepared PCP, where the DI water is in the middle of DC 550 silicone oil (bottom) and PMX 200 silicone oil (top). The selection of the filling liquids should meet the requirements of high light transmittance, immiscibility and refractive indices/density matching. The density of the PMX 200 is lightest, 913 kg/m^3, the density of DI water is 1000 kg/m^3 and the DC 550 silicone oil is heaviest, 1068 kg/m^3. The refractive indices of the three liquids are 1.39 (PMX-200), 1.333 (DI water) and 1.49 (DC 550). Due to the small interfacial tension between DI water and silicone oil (44 mN/m in DI water/PMX 200 interface and 45 mN/m in DI water and DC 550 interface), the initial contact angles of the DI water on the Teflon coated side wall is in the superhydrophobic range ~ 152°. Copper tapes are connected to the left, right and back wall ITO electrodes for connecting to the DC output voltage. Figure 4b illustrates the definition of the prism angle. On the left wall, the contact line of the Teflon/DI water/PMX 200 forms the prism angle θ_1, while the water contact angle in the Teflon/DI water/DC 550 is defined as θ_1'. The two angles on the right wall are defined as θ_2 and θ_2', respectively. It is noteworthy that the initial prism angle θ_1 and θ_2 slightly differ with each other due to the difference of interfacial tension between PMX 200/DI water and DI water/DC 550. Initially, the meniscus presented as dash line is the same as the experimental captured image in Figure 4a. When V_L and V_R are applied to the left and right walls, the prism angles are modified following the Young-Lippmann equation:

$$\theta = \cos^{-1}[\cos(\theta_0) + \frac{\varepsilon_0 \varepsilon_r}{2\gamma_{LV} d} V^2] \quad (1)$$

In which θ is the modified prism angle, θ_0 is the initial prism angle, ε_0 is the vacuum permittivity, ε_r is the relative permittivity of the Teflon AF layer, d is the Teflon AF layer thickness, γ_{LV} is the oil-water interfacial tension and V is the potential difference applied between the side wall electrode and ground electrode. In Equation (1), it is seen the modified prism angle decreases with the increase of the applied potential difference V. At the same time, the modified prism angle is also affected by the relative permittivity and thickness of the dielectric layer, as well as the interfacial tension between water and the surrounding liquid. Figure 4c shows the relationship between prism angle θ_1 and the potential difference between the left side wall electrode and water. Figure 4d shows the scenario on the right wall and the prism angle θ_2. It is seen that both θ_1 and θ_2 reduce with the increase of the applied potential on the left and right wall electrodes. As shown in the inset of Figure 4c, when a potential difference of 138.3 V was applied between left wall and water, an obtuse angle was obtained and the water shape becomes trapezoid. If an equal potential difference of 141.9 V is applied between left wall and water as well as right wall and water, a straight water and oil interface (θ_1=90°) is achieved. If the potential difference between left wall and water increases to 182.8 V, θ_1 changes from the initial obtuse angle to be an acute angle (77.6°). In this case a flipped trapezoid water shape is achieved as shown in the inset of Figure 4c. The scenario in Figure 4d is the same as Figure 4c, except that the modification of prism angle is on the right wall. The water could be tuned as a trapezoid shape as shown in the inset of Figure 4d. The details of the TENG triggered programmable compound prism angle modulation as well as a TENG driven conventional single prism could be found from Supplementary Movie 1.

To utilize the PCP for beam steering, the water and oil interface should be straight so that the beam shines on any point of the interface would undergo the same refraction process. In order to achieve a straight oil/water interface, the potential difference applied on the left side and right side walls should ensure the sum of prism angle meets the relationship of $\theta_1+\theta_2$=180°. When summing up the values on the horizontal ordinate of Figure 4c and 4d, the result always equals to 180°. In each pair of data, the potential difference applied on the left and right electrodes could be read out from the values on the vertical ordinates. The modulation of prism angle θ_1' and θ_2' are similar to θ_1 and θ_2 as the same potential difference are applied to the left and right walls. A slight difference (less than 1°) is caused by the different interfacial tension between PMX 200/DI water and DI water/DC 550 interfaces. This section shows the relationship between prism angle and applied potential difference, as well as the strategy to achieve a straight interface. From the results of TENG output with a RC circuit, the potential difference applied to the prism wall could be varied by changing the resistance in the RC circuit, so that the prism angle could be controlled in a programmable manner with desired water shape.

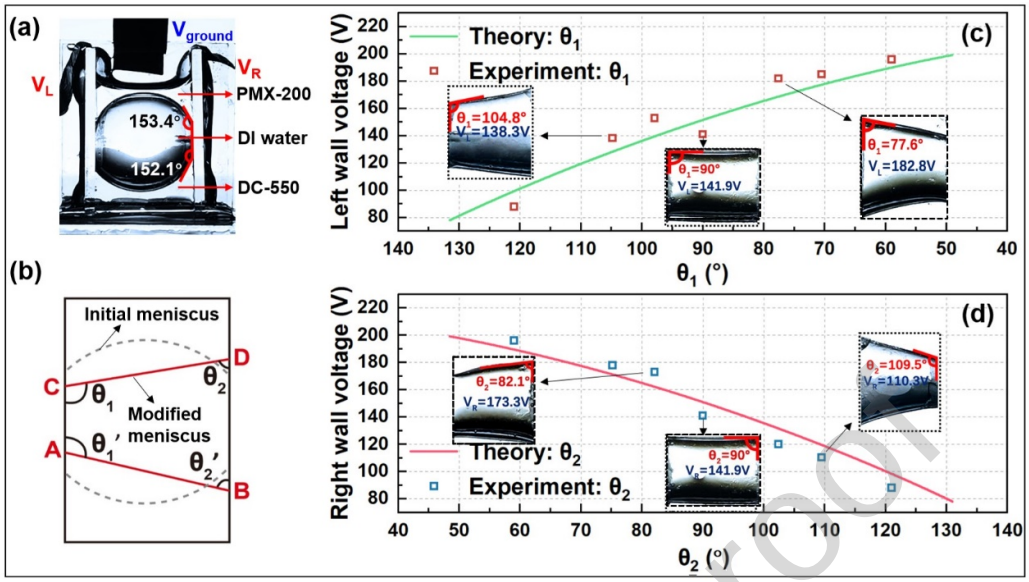

Figure 4 Modulation of prism angle in PCP. (a) Image of an as prepared PCP filled with PMX-200 silicone oil, DI water and DC-550 oil. (b) Definition of the prism angle in PCP. (c) Relationship between the applied DC voltage on the left wall (V_L) and prism angle θ_1. (d) Relationship between the applied DC voltage on the right wall (V_R) and prism angle θ_2.

2.3 Beam steering achieved by the TENG-PCP

With the programmable control function of the prism angle, the PCP could be employed for beam steering. Figure 5a shows an experimental setup for deflecting a laser beam by the PCP. In this setup, a vertical laser beam is employed to shine on the PCP from bottom and the deflection angle β could be determined by the distance between the initial and deflected spot position (d) divided by the distance between PCP and screen (h): $\beta=arctan(d/h)$. Details of the TENG triggered PCP for beam steering could be found from Supplementary Movie 2. As the light path is reversible, the oblique incident solar beam shining from the top of the prism could be deflected vertically to the concentrating optics.

In order to distinguish the beam steering performance between the presented PCP and the conventional single prism with only a pair of liquids, the light paths in these two prisms are shown in Figure 5b. In the single prism, the immiscible liquids are DC 550 oil and DI water, the only difference in PCP is an extra PMX 200 silicone oil on top of the DI water. It is noteworthy that the combination of DC 550 oil and DI water is the best among the three liquids as the difference of refractive index between the two liquids is the largest (DC 550:1.49, DI water: 1.333). When a vertical laser beam enters the two prisms, the light path in DC 550 oil and DI water would be the same. The only difference in the PCP is that the beam I_2 in the DI water would enter PMX 200 before exiting the prism. In the DI water and PMX 200 interface, if the refractive indices of the two liquids are identical, the beam will not be deflected and propagate along the red dash line in the PMX 200. But in the real case, the refractive index of PMX 200 is 1.39, which is greater than DI water, so the refraction angle β_2 is smaller than the incident angle α_2 according to the Snell's law. The beam I_3 in the PCP would

be deflected an angle of α_2-β_2 more than the beam in the single prism before exiting the prism. By theoretical derivation, the deflection angles in single prism and in PCP can be expressed by (2) and (3). When the prism angle is in the range of 90°-180°, the deflection angle in PCP (β_{PCP}) is always greater than the deflection angle in single prism (β_{single}). The detailed derivation process could be found from Supporting Information.

$$\beta_{\text{single}} = \arcsin(n_2 \sin(\arcsin(\frac{n_1}{n_2}\sin(\theta_2^{'} - 90) + 90 - \theta_2^{'}))) \quad (2)$$

$$\beta_{PCP} = \arcsin(n_3 \sin(\theta_2^{'} - 90 - \arcsin(\frac{n_2}{n_3}(2\theta_2^{'} - 180 - \arcsin(\frac{n_1}{n_2}\sin(\theta_2^{'} - 90)))))) \quad (3)$$

The experimental results proved the theoretical prediction. Figure 5c presents the beam deflection of a vertical laser beam by PCP and single prism. When the prism angle $\theta_2^{'}$ equals to 60° and 120°, the PCP could deflect the vertical laser beam from initial point to a negative 18 mm and positive 16 mm. As a comparison, the single prism deflects the vertical laser beam to a negative 13 mm and positive 10 mm from initial point. This indicates that the TENG-PCP could deflect the solar beam with a wider incident angle range, as compared to the single prism.

The experimental tested deflection angles of the single prism and PCP are plotted in Figure 5d, where a larger deflection angle is achieved by the PCP (red line) as compared to the single prism (green line). The measured deflection angle (empty square) well agrees with the theoretical calculation in the PCP. A maximum improvement of ~38% was achieved when the prism angle $\theta_2^{'}$ equals 60°. Figure 5e presents the reflection loss of the light intensity at each interface. The reflection loss could be calculated based on Fresnel's equations (4-6):

$$R_{eff} = \frac{1}{2}(R_S + R_P) \quad (4)$$

$$R_S = \left|\frac{n_1\cos(\theta_i) - n_2\cos(\theta_t)}{n_1\cos(\theta_i) + n_2\cos(\theta_t)}\right|^2 \quad (5)$$

$$R_P = \left|\frac{n_1\cos(\theta_t) - n_2\cos(\theta_i)}{n_1\cos(\theta_t) + n_2\cos(\theta_i)}\right|^2 \quad (6)$$

In which R_{eff} is the effective reflectance, R_{S} is the reflectance for s-polarized light, R_{P} is the reflectance for p-polarized light, θ_{i} is the incident angle at each interface and θ_{t} is the refraction angle. Due to the existence of PMX 200/DI water interface in the PCP, the reflection loss is greater in PCP (R_1+R_2+R_3) than in single prism (R_1+R_2). When the prism angle equals 60°, the reflection loss in PCP is 3.2%, while a 2.4% reflection loss is achieved in the single prism.

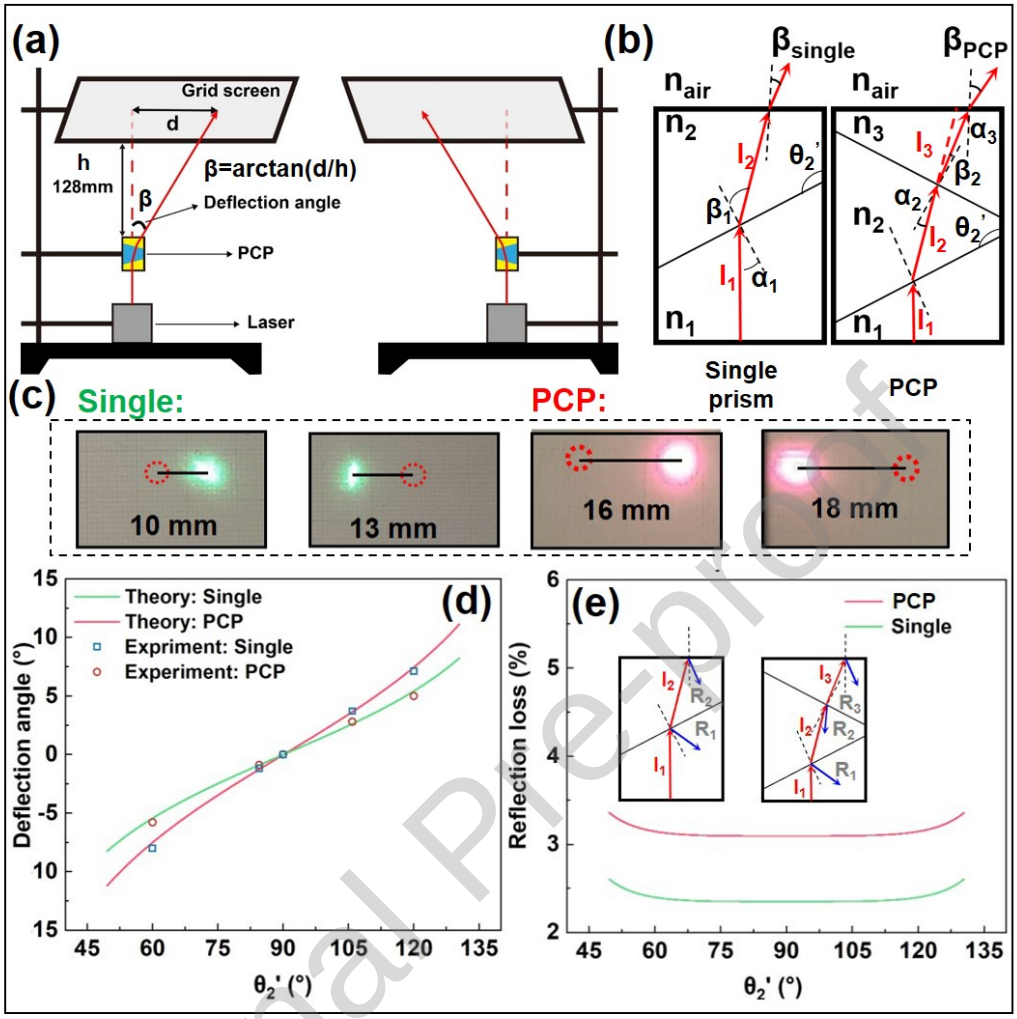

Figure 5 Beam steering performance of the PCP. (a) Schematic image showing the setup for beam deflection. (b) Comparison of light path in PCP and single prism. (c) Experimental captured image of a deflected beam from positive and negative incident angles in PCP and single prism. (d) Relationship between the deflection angle β and prism angle θ_2'. (e) Relationship between the reflection loss and prism angle θ_2'.

2.4 Demonstration of beam steering in the concentrator photovoltaics

Figure 6 presents the beam steering performance of PCP for CPV applications. Prior to the experimental test, a numerical simulation is conducted to examine the pathways of oblique and perpendicular incident beams after passing through the concentrating Fresnel lens. As shown in Figure 6a, the oblique incident beam shining to the Fresnel lens was failed to be concentrated and the outgoing beam was off the stationary screen. However, if a perpendicular light beam is shining to the Fresnel lens, the beam is concentrated to the center of the screen by the Fresnel lens. Imagine that if the screen is replaced by the multi-junction cell, the oblique incident solar beam will miss the solar cell and will not produce electricity. An experimental demonstration further verifies this concept as shown in Figure 6c and 6d. An oblique incident beam with incident angle of -8° is shined to the PCP. As the TENG is not turned on in Figure 6c, the light beam after passing the PCP and Fresnel lens miss the target of multi-junction

solar. The multimeter in Figure 6c shows a reference data of 0.918 V which is generated by the environment light. However, if the TENG is turned on and a left wall voltage of 88 V and right wall voltage of 197 V are applied to the PCP, a prism angle of θ_2=60° is induced and the laser beam is deflected to be on target of the multi-junction cell and a 2.301 V voltage was attained by the multimeter. With the operation of TENG-PCP, the increment of the solar cell output was 1.2 mW (0.088 mW of reference data and 1.288 mW with the deflected laser beam). The result indicates that by the input power from TENG which could be operated by environmental energy, the CPV output power could be boosted significantly. The light path before and after the operation of TENG-PCP is presented in the inset of Figure 6. Detailed information of the demonstration of using TENG-PCP for CPV application as well as the light path modulation could be found from Supplementary Movie 3.

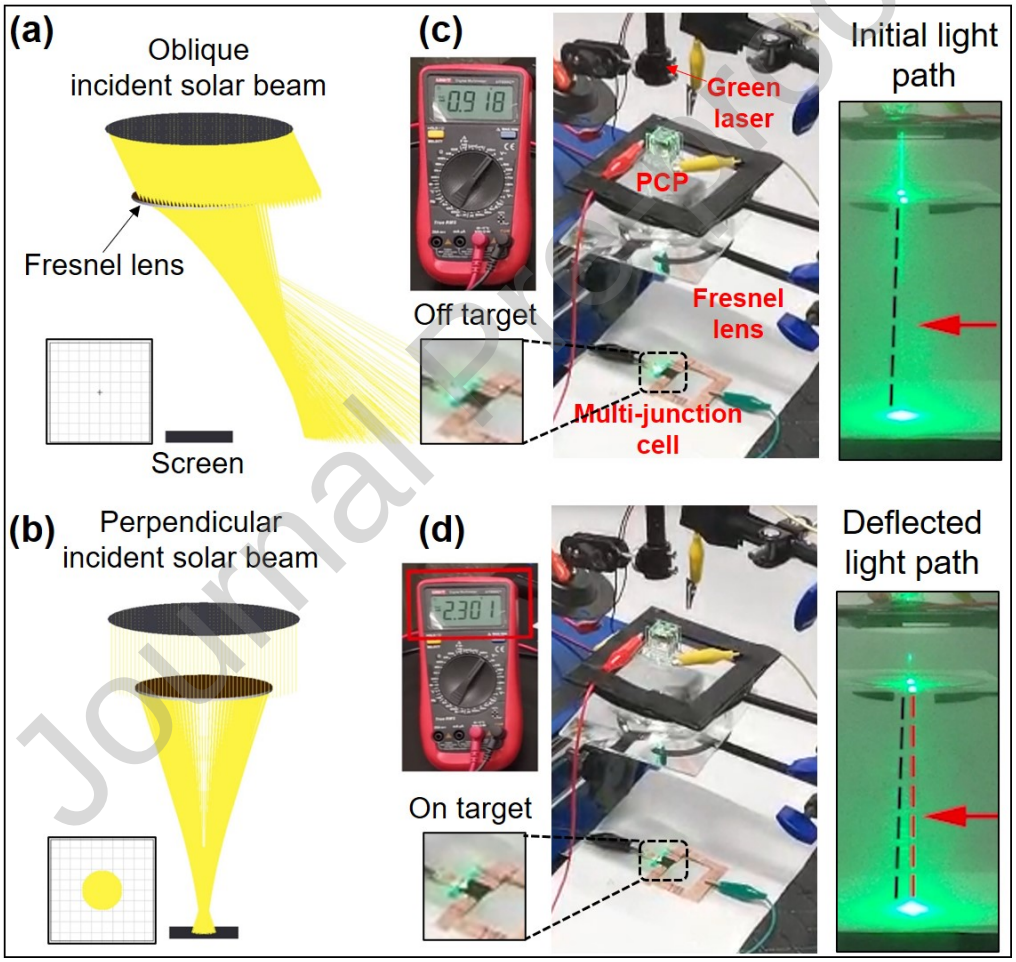

Figure 6 Demonstration of beam steering for the application in CPV. (a) and (b) Numerical simulation of oblique and perpendicular incident beam passing through a concentrating Fresnel lens. (c) Experimental demonstration of a laser beam shining to a PCP without power supply and the laser beam misses the multi-junction solar cell after the Fresnel lens. The multimeter connecting with the solar cells shows a reference voltage of 0.918 V. (d) Experimental demonstration of a laser beam shining to a PCP with left wall voltage of 88 V, right wall voltage of 197 V. The laser beam

was deflected to be perpendicularly shining to the Fresnel lens and the light spot is concentrated to the multi-junction solar cell, yielding a 2.301 V voltage on the multimeter. Inset of Figure 6 shows the light pathway before and after the operation of TENG powered PCP.

It is noteworthy the demonstration of beam steering of PCP is achieved by a step motor driven disc TENG in the current study. In real applications, the driving of the disc TENG is expected to be achieved by renewable and environmental energy sources including wind, water wave and even human body motion. Since various high performance wind, water wave and human motion triggered TENGs [52-57] are developed in recent years, the TENG-PCP is expected to be integrated with these TENGs for pursuing an environmental-friendly solar beam steering device.

Conclusion

This work presents a TENG powered programmable compound prism for solar beam steering. A RC circuit is employed for converting the AC output signal from TENG into DC signal. By changing the resistance in the circuit, varied DC outputs range from 88–197 V were attained. The obtained DC output voltage was utilized for modifying the meniscus between PMX 200 silicone oil and DI water as well as DI water and DC 550 oil in a compound prism. Following the prediction of Young-Lippmann equation, the meniscus and prism angle are continuously tuned by varying the applied DC voltage, which provides the compound prism a programmable feature. A smallest prism angle (θ_1 or θ_2) of 60° was achieved when DC voltage of 197 V and 88 V were applied to the left or right walls. Such a prism angle is able to deflect a light beam with an incident angle range of 15° to be perpendicular to the Fresnel lens, which is 38% greater than the conventional single prism with only a pair of immiscible liquids. The proposed TENG-PCP was demonstrated to deflect an oblique incident laser beam, and the perpendicular outgoing beam successfully spots on the multi-junction solar cell to boost the output power from 0.088 mW to 1.288 mW by solar cell.

Materials and Methods

*Device fabrication***.** The TENG is assembled by a circle-shaped acrylic cover (20 cm in diameter), a half circle-shaped FEP thin film (with diameter of 20 cm and thickness of 50 μm), a pair of half circle-shaped copper electrodes (with diameter of 20 cm and thickness of 50 μm), and an acrylic substrate (with the same dimension of the acrylic cover). The FEP film is stick to the acrylic cover, while the two copper electrodes were stick to the acrylic substrate. The acrylic cover serves as a rotor and is driven by a step motor, while the substrate serves as stator. The PCP is assembled by three pieces of ITO glass which form the left, right and back walls of the prism, and two pieces of bare glass that form the front and base of the prism. Prior to the prism assemble, the left, right, front and back walls of the prism were spin-coated with a Teflon AF solution. The Teflon AF solution was prepared by dissolving commercial

Teflon AF1601X powder with FC-40 (3M products) at 60°C at a concentration of 5%.

After baking in the oven for 10 mins at 120°C and 20 mins at 170°C, a 5.5 μm thin film is coated to the surface of the four glass walls. The middle of the back wall was cut for a hole for short-connecting with DI water. The five pieces of glass were stick by optical epoxy to form a container. Copper wires were connected to the left, right and back walls for the connection of DC signal. DC 550 oil (Dow Corning), DI water and PMX 200 oil (Dow Corning) were injected into the prism by pipette with a volume rate of 10:6:3.

*Characterization***.** The output performance of the TENG and modulated DC signal were measured by Keithley 6514 electrometer. The meniscus of the oil/water interface was characterized by a CCD camera and the contact angle was evaluated by an open-source software ImageJ. The distance of the deflected beam from initial position was measured by a coordinate sheet. The output performance of the multi-junction cell was measured by a commercial multimeter.

*Numerical simulation***.** The pathways of oblique and perpendicular incident beams are simulated by Optic Studio 13.0. A built-in Fresnel lens with a focal length of 194 mm is employed and 100 parallel rays are modelled for ray tracing in after passing the Fresnel lens.

Acknowledgements

This work was supported by National Natural Science Foundation of China (51906031) and Fundamental Research Funds for the Central Universities, DUT20LAB105.

References

[1] R. R. King, Nat. Photonics 2 (2008) 284.
[2] P. Pérez-Higueras, E. Muñoz, G. Almonacid, and P. Vidal, Renew. Sust. Energy Rev. 15 (2011) 1810-1815.
[3] M. A. Green and S. P. Bremner, Nat. Mater. 16 (2016) 23-34.
[4] Z. Wang, Q. Lin, B. Wenger, M. G. Christoforo, Y. H. Lin, M. T. Klug, M. B. Johnston, L. M. Herz, and H. J. Snaith, Nat. Energy 3 (2018) 855-861.
[5] H. Cotal, C. Fetzer, J. Boisvert, G. Kinsey, R. King, P. Hebert, H. Yoon, and N. Karam, Energy Environ. Sci. 2 (2009) 174-192.
[6] R. Moon, L. James, H. Vanderplas, Y. Chai, and G. Antypas, "13th IEEE Photovoltaic Specialist Conference," ed: Washington, DC (IEEE, New York, 1978), 1975.
[7] S. Bedair, M. Lamorte, and J. Hauser, Applied Physics Letters 34 (1979) 38-39.
[8] M. A. Green, Y. Hishikawa, W. Warta, E. D. Dunlop, D. H. Levi, J. Hohl-Ebinger, and A. W. Ho-Baillie, Prog. Photovoltaics 25 (2017) 668-676.
[9] M. A. Green, Phys. Today 57 (2004) 71-72.
[10] K. Shanks, S. Senthilarasu, and T. K. Mallick, Renew. Sust. Energy Rev. 60 (2016) 394-407.
[11] W. Wang, C. Li, H. Rodrigue, F. Yuan, M.-W. Han, M. Cho, and S.-H. Ahn, Adv. Func. Mater. 27 (2017) 1604214.

[12] H. Mousazadeh, A. Keyhani, A. Javadi, H. Mobli, K. Abrinia, and A. Sharifi, Renew. Sust. Energy Rev. 13 (2009) 1800-1818.
[13] J. S. Price, X. Sheng, B. M. Meulblok, J. A. Rogers, and N. C. Giebink, Nat. Comm. 6 (2015) 6223.
[14] F. Meinardi, F. Bruni, and S. Brovelli, Nature Reviews Materials 2 (2017) 17072.
[15] I. Luque-Heredia, G. Quéméré, R. Cervantes, O. Laurent, E. Chiappori, and J. Y. Chong, "The sun tracker in concentrator photovoltaics," in *Next Generation of Photovoltaics*: Springer, 2012, pp. 61-93.
[16] S. Smith and M. Shiao, Solar Market Research (2012) 2013-2016.
[17] H. Apostoleris, M. Stefancich, and M. Chiesa, Nat. Energy 1 (2016) 16018.
[18] D. Erickson, D. Sinton, and D. Psaltis, Nat. Photonics 5 (2011) 583-590.
[19] J. Cheng, S. Park, and C. L. Chen, Sol. Energy 89 (2013) 152-161.
[20] S. K. Thio, D. Jiang, and S.-Y. Park, Lab Chip 18 (2018) 1725-1735.
[21] J. Cheng and C.-L. Chen, Appl. Phys. Lett. 99 (2011) 191108.
[22] V. Narasimhan, D. Jiang, and S.-Y. Park, Appl. Energy 162 (2016) 450-459.
[23] F.-R. Fan, Z.-Q. Tian, and Z. L. Wang, Nano Energy 1 (2012) 328-334.
[24] Z. L. Wang, Mater. Today 20 (2017) 74-82.
[25] Z. L. Wang and A. C. Wang, Mater. Today 30 (2019) 34-51.
[26] Y. Xi, H. Guo, Y. Zi, X. Li, J. Wang, J. Deng, S. Li, C. Hu, X. Cao, and Z. L. Wang, Adv. Energy Mater. 7 (2017) 1602397.
[27] W. Liu, Z. Wang, G. Wang, Q. Zeng, W. He, L. Liu, X. Wang, Y. Xi, H. Guo, C. Hu, and Z. L. Wang, Nat. Comm. 11 (2020) 1883.
[28] S. Chatterjee, S. R. Burman, I. Khan, S. Saha, D. Choi, S. Lee, and Z.-H. Lin, Nanoscale 12 (2020) 17663-17697.
[29] J. Chen, J. Yang, Z. Li, X. Fan, Y. Zi, Q. Jing, H. Guo, Z. Wen, K. C. Pradel, S. Niu, and Z. L. Wang, ACS Nano 9 (2015) 3324-3331.
[30] M. Xu, T. Zhao, C. Wang, S. L. Zhang, Z. Li, X. Pan, and Z. L. Wang, ACS Nano 13 (2019) 1932-1939.
[31] Z. Wen, Y. Yang, N. Sun, G. Li, Y. Liu, C. Chen, J. Shi, L. Xie, H. Jiang, D. Bao, Q. Zhuo, and X. Sun, Adv. Func. Mater. 28 (2018) 1803684.
[32] D. Jiang, M. Xu, M. Dong, F. Guo, X. Liu, G. Chen, and Z. L. Wang, Renew. Sust. Energy Rev. 115 (2019) 109366.
[33] W. Liu, Z. Wang, G. Wang, G. Liu, J. Chen, X. Pu, Y. Xi, X. Wang, H. Guo, C. Hu, and Z. L. Wang, Nat. Comm. 10 (2019) 1426.
[34] W. He, W. Liu, J. Chen, Z. Wang, Y. Liu, X. Pu, H. Yang, Q. Tang, H. Yang, H. Guo, and C. Hu, Nat. Comm. 11 (2020) 4277.
[35] Y. Liu, W. Liu, Z. Wang, W. He, Q. Tang, Y. Xi, X. Wang, H. Guo, and C. Hu, Nat. Comm. 11 (2020) 1599.
[36] L. Gao, X. Chen, S. Lu, H. Zhou, W. Xie, J. Chen, M. Qi, H. Yu, X. Mu, Z. L. Wang, and Y. Yang, Adv. Energy Mater. 9 (2019) 1902725.
[37] Y. Xie, S. Wang, L. Lin, Q. Jing, Z.-H. Lin, S. Niu, Z. Wu, and Z. L. Wang, ACS Nano 7 (2013) 7119-7125.
[38] G. Cheng, Z.-H. Lin, Z.-l. Du, and Z. L. Wang, ACS Nano 8 (2014) 1932-1939.
[39] H. Zhang, Y. Yang, T.-C. Hou, Y. Su, C. Hu, and Z. L. Wang, Nano Energy 2 (2013) 1019-1024.
[40] J. Nie, X. Chen, and Z. L. Wang, Adv. Func. Mater. 29 (2018) 1806351.
[41] H. Yang, Y. Pang, T. Bu, W. Liu, J. Luo, D. Jiang, C. Zhang, and Z. L. Wang, Nat. Comm. 10 (2019) 2309.
[42] Y. Zi, S. Niu, J. Wang, Z. Wen, W. Tang, and Z. L. Wang, Nat. Comm. 6 (2015) 8376.
[43] J. Hu, X. Pu, H. Yang, Q. Zeng, Q. Tang, D. Zhang, C. Hu, and Y. Xi, Nano Res. 12 (2019) 3018-3023.
[44] H. Yang, M. Deng, Q. Tang, W. He, C. Hu, Y. Xi, R. Liu, and Z. L. Wang, Adv. Energy Mater. 9 (2019) 1901149.

[45] X. Pu, H. Guo, J. Chen, X. Wang, Y. Xi, C. Hu, and Z. L. Wang, Sci. Adv. 3 (2017) e1700694.
[46] G. Hengyu, P. Xianjie, C. Jie, M. Yan, Y. Min-Hsin, L. Guanlin, T. Qian, C. Baodong, L. Di, and Q. Song, Sci. Robot. 3 (2018) eaat2516-.
[47] J. Wang, H. Wang, X. Li, and Y. Zi, Nano Energy 66 (2019) 104140.
[48] C. Fang, Y. Cao, D. Jiang, J. Tian, and C. Zhang, Microsyst. Nanoeng. 6 (2020).
[49] X. Chen, X. Pu, T. Jiang, A. Yu, L. Xu, and Z. L. Wang, Adv. Func. Mater. 27 (2017) 1603788.
[50] C. Zhang, Z. Guo, X. Zheng, X. Zhao, H. Wang, F. Liang, S. Guan, Y. Wang, Y. Zhao, A. Chen, G. Zhu, and Z. L. Wang, Adv. Mater. 32 (2020) e1904988.
[51] X. Chen, Y. Wu, A. Yu, L. Xu, L. Zheng, Y. Liu, H. Li, and Z. Lin Wang, Nano Energy 38 (2017) 91-100.
[52] S. Cho, Y. Yun, S. Jang, Y. Ra, J. H. Choi, H. J. Hwang, D. Choi, and D. Choi, Nano Energy 71 (2020) 104584.
[53] S. Choi, S. Cho, Y. Yun, S. Jang, J. H. Choi, Y. Ra, M. La, S. J. Park, and D. Choi, Adv. Mater. Tech. 5 (2020) 2070023.
[54] D. Choi, S. Lee, S. M. Park, H. Cho, W. Hwang, and D. S. Kim, Nano Res. 8 (2015) 2481-2491.
[55] T. Kim, J. Chung, D. Y. Kim, J. H. Moon, S. Lee, M. Cho, S. H. Lee, and S. Lee, Nano Energy 27 (2016) 340-351.
[56] H. Yong, J. Chung, D. Choi, D. Jung, M. Cho, and S. Lee, Sci. Rep. 6 (2016) 33977.
[57] Z. Zhao, X. Pu, C. Du, L. Li, C. Jiang, W. Hu, and Z. L. Wang, ACS Nano 10 (2016) 1780-7.

Guijun Chen is an Associate Professor in Dalian University of Technology. He is working on the modelling and analysis of thermal energy systems hydrodynamics including boilers, heat exchangers, recycling of condensate water and so on.

Yutao Wang received his Bachelor's degree in North China Electric Power University. Now he is a Master candidate in Prof. Dongyue Jiang and Prof. Guijun Chen's group in Dalian University of Technology. His research interests include triboelectric nanogenerators and liquid actuators.

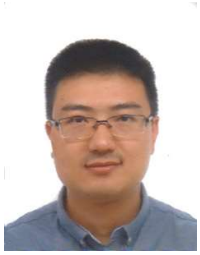

Dongyue Jiang received his Ph.D degree in National University of Singapore. Now he is an Associate Professor at Dalian University of Technology. His research interests include: triboelectric nanogenerators, multi-phase flow, EWOD as well as their applications in renewable and sustainable systems.

Hongchen Wang received his Bachelor's degree in Changsha University of Science & Technology. Now he is a Master candidate under supervision of Prof. Dongyue Jiang in Dalian University of Technology. His research interests include triboelectric nanogenerators, gradient surface and liquid actuators.

Kun Wang received his Bachelor's degree in Shandong University of Technology. Now he is a Master candidate in Prof. Dongyue Jiang and Prof. Guijun Chen's group in Dalian University of Technology. His research interests include hydrogel, two phase flow and triboelectric nanogenerators.

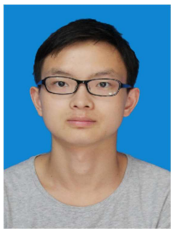

Jie Tan received his Bachelor's degree in Wuhan Institute of Technology. Now he is a Master candidate in Prof. Dongyue Jiang and Prof. Guijun Chen's group. His research interests include controllable droplet impact behaviour and triboelectric nanogenerators.

Mingyang Sun received his Bachelor's degree in Shandong Jianzhu University. Now he is a Master candidate in Prof. Dongyue Jiang and Prof. Guijun Chen's group. His research interests include phase change thermal storage and triboelectric nanogenerators.

Yongchen Song is a Full Professor, vice President of Dalian University of Technology, Director of Key Laboratory of Ocean Energy Utilization and Energy Conservation of Ministry of Education. His research interests includes Methane hydrate and ocean energy utilization.

Minyi Xu received his Ph.D degree from Peking University. During 2016-2017, he joined Professor Zhong Lin Wang's group at Georgia Institute of Technology. Now he is a Full Professor in Dalian Maritime University. His research interests include blue energy, self-powered systems, triboelectric nanogenerators and its applications in smart ship and ocean.

Credit Author Statement

Guijun Chen: Conceptualization;

Yutao Wang: Investigation, Software;

Dongyue Jiang: Writing- original draft preparation;

Hongchen Wang: Investigation;

Kun Wang: Methodology;

Jie Tan: Software;

Mingyang Sun: Investigation;

Yongchen Song: Writing- Reviewing and Editing;

Minyi Xu: Writing- Reviewing and Editing.

Declaration of interests

☒ The authors declare that they have no known competing financial interests or personal relationships that could have appeared to influence the work reported in this paper.

☐The authors declare the following financial interests/personal relationships which may be considered as potential competing interests:

Research Highlights

The adoption of TENG eliminates the dependence of bulky DC power sources.

The proposed PCP shows a 38% greater deflection angle than conventional single prism.

The solar cell output power was boosted from 0.088 mW to 1.288 mW by TENG-PCP.